Supplementary Information

Programmable dynamic interfacial spinning of bioinspired microfibers with volumetric encoding

Ming Zhang, Shiyu Wang, Yuanqing Zhu, Zhiqiang Zhu, Ting Si,* and Ronald X. Xu**

Mr. M. Zhang, Mr. S. Y. Wang, Mr. Y. Q. Zhu, Dr. Z. Q. Zhu, Prof. R. X. Xu
Key Laboratory of Precision Scientific Instrumentation of Anhui Higher Education Institutes
Department of Precision Machinery and Precision Instrumentation
University of Science and Technology of China
Hefei 230026, China
E-mail: zqzhu2017@ustc.edu.cn

Prof. R. X. Xu
Department of Biomedical Engineering
The Ohio State University
Columbus, Ohio 43210, USA
E-mail: xu.202@osu.edu

Prof. T. Si
Department of Modern Mechanics
University of Science and Technology of China
Hefei 230026, China
E-mail: tsi@ustc.edu.cn

Keywords: encoded microfiber, embedded droplet, interfacial spinning, information encryption, drug release

Materials

Sodium alginate (Na-Alg, medium viscosity), polyvinyl alcohol (PVA, Mw 13000-23000, 87-89% hydrolyzed), trimethylolpropane ethoxylate triacrylate (ETPTA), 2-hydroxy-2-methylpropiophenone (HMPP) and 1,1,1,2,3,4,4,5,5,5-decafluoropentane (HFC) were all purchased from Sigma-Aldrich. Calcium chloride and acetone were supplied by Sinopharm Chemical Reagent Co., Ltd. Fluorescent polystyrene nanoparticles (excitation/emission: 570/610 nm) were bought from Baseline. Coumarin 6 and Nile red were purchased from Aladdin and Ekear, respectively. Magnetic Fe_3O_4 nanoparticles (MNPs, 20nm) were supplied by Macklin. Commercial security printing inks with UV or temperature responsiveness were purchased from Aobo Security Technology Co., Ltd. Deionized water was produced by Millipore Direct-Q system. The outer aqueous solution was prepared by mixing 0.5 wt% Na-Alg, 1 wt% PVA and 0.04 wt% fluorescent polystyrene nanoparticles. ETPTA with 2 wt% HMPP, 50 wt% security printing inks dissolved in acetone and HFC were separately applied as the inner phase for the generation of droplet-embedded microfibers. 0.5 wt% calcium chloride was dissolved in ddH_2O to serve as gelation bath for fiber spinning.

Fabrication of the spinning device for dynamic interfacial spinning (DIS)

In DIS process, the spinning nozzles consisted of common stainless needles and could be readily constructed without the help of expensive microfabrication equipment, which brought in the advantages of low cost and simple manufacturing over the tapered capillaries or microfluidic chips applied in traditional microfluidic spinning technology (MST). For the

generation of bioinspired droplet-embedded microfibers, the spinning nozzle was assembled using an outer 21G stainless needle and a coaxially inserted 30G inner needle (Figure S1). The assembled nozzle was then sealed by ultraviolet (UV)-curing glue and immobilized under UV irradiation. To construct the spinning nozzle for microfibers with inner structure of dual droplets, two 34G stainless needles were parallelly arranged within an outer 17G needle at a distance of 310 μm to avoid the contact of inner fluids during fiber spinning. In contrast, the dual 34G inner needles were fixed closely for the generation of microfibers with embedded Janus droplets. Moreover, an outer 18G needle, a middle 22G needle and an inner 30G needle were assembled together to serve as the spinning nozzle for the generation of microfibers with embedded core-shell capsules (Figure S8).

Fiber spinning through DIS process

In a typical DIS system, the vibration action was exerted on the spinning nozzle through an electromagnetic exciter (SA-JZ002, Shiao technology Co., Ltd). To control the vibration parameters of electromagnetic exciter, a tunable waveform signal was created by a programmable generator (DG1022U, Rigol) and then enhanced through a power amplifier (SA-PA010, Shiao technology Co., Ltd) to be input to the exciter. When generating droplet-embedded microfibers, the outer phase of 0.5 wt% Na-Alg solution and inner phase of ETPTA with 2 wt% HMPP as photoinitiator were separately pumped into corresponding channels of the spinning nozzle through syringe pumps (LSP02-2A, Longerpump). Meanwhile, the orifice of spinning nozzle was immersed in 0.5 wt% $CaCl_2$ solution. When a sine waveform was

generated as the input signal to the exciter, the resultant vibration amplitude and frequency of spinning nozzle were manipulated by adjusting the signal level and period, respectively. To control the deformation degree of resultant microfibers, the shearing height *H* was manipulated by adjusting the height of lifting platform, where the coagulation bath was placed. Alternatively, the adjustment of vibration amplitude also could achieve precise control of *H*. The produced microfibers were collected in a glass petri dish with 0.5 wt% $CaCl_2$ solution and then irradiated in an ultraviolet (UV) curing box (Intelli-Ray 400, Uvitron). To investigate the morphology evolution of hydrogel microfibers with varying concentration of alginate solution and $CaCl_2$ bath, a uniaxial 21G stainless needle was utilized as the spinning nozzle to eliminate the influence of inner fluid on the fiber deformation.

Volumetric encoding of droplet-embedded microfibers through programmable DIS

Prior to the generation of volume-encoded microfibers, a programmed waveform signal was edited on the waveform generator to replace the aforementioned sine waves. In general, the programmed waveforms consisted of consecutive triangular waves, which were arranged at different interval time *T* based on the ASCII codes of customized information. After the programmed waveform signals were input to the exciter during fiber spinning, two kinds of vibration interval time (T = 125, 500 ms) were generated for the spinning nozzle, leading to the formation of binary inner encoding droplets with sufficient volume difference. Through reprogramming the input waveforms with additional internal time, more encoding units could be incorporated within the produced microfibers to improve the encoding efficiency. For the

generation of volume-encoded microfibers with ETPTA inner beads, 0.04 wt% fluorescent polystyrene nanoparticles and coumarin 6 were separately added into the outer and inner fluid to facilitate the fluorescent characterization of resultant microfibers. The generated volume-encoded microfibers with stored information were irradiated by UV light and collected in a petri dish for subsequent tests.

Construction of two-dimensional networks for information encryption

In order to generate volume-encoded microfibers with stimuli responsiveness, two kinds of inner solution were prepared through the mixing of commercial security printing inks, acetone, and Span 80 (volume ratio = 6 : 4 : 1), which were then pumped into the inner channel of coaxial spinning nozzle. After that, UV-responsive microfibers encoded with letter U and temperature-responsive microfibers encoded with letter T were separately generated applying corresponding programmed input signals. The resultant volume-encoded microfibers were then collected in glass petri dishes with 0.5 wt% $CaCl_2$ solution. The UV responsiveness of volume-encoded microfibers was tested utilizing UV irradiation from an area light source, while the temperature responsiveness was verified through heating the collection petri dish on a constant temperature magnetic stirrer (B11-3, Shanghai Sile Instruments Co., LTD). For the construction of two-dimensional encrypted networks, UV-responsive and temperature-responsive volume-encoded microfibers were generated and then blended on a petri dish for following decryption.

Construction of functionalized volume-encoded microfibers for potential controllable drug release

To endow volume-encoded microfibers with the application potential for controllable drug release in blood vessels, 4 wt% MNPs was added into the outer Na-Alg solution while HFC was applied as the inner phase. The on-demand excitation of embedded HFC droplets in resultant microfibers was implemented utilizing a near-infrared (NIR) laser device (FU808ADX-F34, Shenzhen Fulei Technology Co., LTD) with a focusing lens. Here, coumarin 6 was added into the inner HFC phase as the model drug. For the construction of customized HFC-embedded microfibers, a programmed vibration mode with three interval time (T = 125, 250, 500 ms) was applied on the coaxial nozzle during fiber spinning. Then, the resultant volume-encoded microfibers with programmed HFC droplet sequence were collected in a petri dish with 0.5 wt% $CaCl_2$ solution for the subsequent excitation.

Characterization

The dynamic interfacial spinning process was monitored by charge-coupled device (CCD, DFK 23G274, Imaginsource) camera and recorded by high-speed camera (Mini AX200, Photron) with the help of microscopic lens. Stereoscopic and fluorescent images were captured using a wide-field stereoscopic microscope (AXIO Zoom.V16, Zeiss). To characterize the macroscopic appearance, single-lens reflex (SLR) camera (D810, Nikon) was employed to snap the images of volume-encoded microfibers. Besides, the controllable excitation process for HFC-embedded microfibers was recorded by stereomicroscope (SZX7, Olympus) equipped

with CCD camera (MSX2-H, Mshot). The decryption process for two-dimensional encrypted network was filmed using SLR camera (D810, Nikon). Size statistics for embedded droplets in generated microfibers was accomplished using software ImageJ.

Three spinning modes in DIS process

For DIS process, there were three spinning modes corresponding to different motion states of the spinning nozzle. When the spinning nozzle was kept motionless and submerged in the coagulating bath, the inner phase of ETPTA passively broke into discrete droplets, due to the shearing effect of outer alginate fluid, as shown in **Figure S14a** (Mode 1). However, when a vertical vibration was applied on the spinning nozzle, the inner ETPTA phase would be actively cut off from the nozzle by interfacial shearing force F_i to form discrete droplets. During the active generation process of embedded droplets, there were two kinds of forces with opposite effects: (1) the interfacial shearing force F_i and the gravity G_D of pendant droplets that intended to make the pendant droplets detach from the spinning nozzle; (2) the capillary force F_c that intended to keep the pendant droplets on the nozzle. As shown in Figure S14c, the inner ETPTA fluid broke up into discrete droplets at a high shearing height H with the droplet generation frequency synchronous with the nozzle vibration, which was due to the adequate F_i derived from the dramatic deformation of the outer hydrogel sheath (Mode 3). When H was relatively low, the sum of the interfacial shearing force F_i and the gravity G_D of pendant droplets was not enough to overcome the capillary force F_c. Under the circumstances, the pendant ETPTA droplets would grow up during multiple vibration rather than being cut off from the nozzle after

every upward vibration. As the volumes of pendant droplets increased, Gravity G_D of the droplet would increase while the capillary force F_c would decrease accordingly, eventually leading to the formation of discrete droplets. Therefore, the vibration frequency of spinning nozzle was an integer multiple of the generation frequency of embedded droplets, as shown in Figure S14b (Mode 2). Apparently, the breaking modes of inner phase could be facilely regulated through adjusting the vibrating motion of spinning nozzle, which enabled the transition from passive generation (Mode 1) to active generation (Mode 2 and 3) of the embedded droplets in deformed microfibers.

To clarify the generation frequency of embedded droplets in different spinning modes, the diameters of embedded droplets in produced microfibers were measured (**Figure S15**). According to Equation 1, the theoretical generation frequency f_g of embedded droplets could be calculated as follows,

$$f_g = 6Q_i/\pi D_i^3, \quad (3)$$

As presented in Figure S15, the value of f_g was consistent with the actual vibration frequency of spinning nozzle (f = 4 Hz) in Mode 3, while f was the double of f_g (2Hz) in Mode 2. Moreover, the theoretical passive generation frequency of embedded droplets in Mode 1 was calculated as 1.20Hz. To further investigate the role of nozzle vibration in DIS process, the vibration frequency f and the shearing height H were separately manipulated to investigate their effects on the spinning modes of droplet-embedded microfibers. As shown in **Figure S16**, it was revealed that the spinning mode in DIS process underwent controllable conversion from asynchronous Mode 2 to synchronous Mode 3 through increasing the shearing height. However,

severe disturbances would be introduced into the spinning system under relatively high *f* and *H*, resulting in the unstable generation of irregular or fractured microfibers with non-uniform embedded droplets (Figure S3). The produced droplet-embedded microfibers were transferred into $CaCl_2$ solution and irradiated by ultraviolet (UV) light so that the embedded ETPTA droplets were solidified into beads. **Figure S17a** exhibited the morphology of the hydrated beads-embedded microfibers generated under three spinning modes, with the outer hydrogel sheath presenting varying degrees of deformation. After dehydration, the outer hydrogel sheath of microfibers would shrink to tightly wrap the embedded beads, as shown in Figure S17b and S16c. Since the droplet-embedded microfibers generated under Mode 3 possessed uniform outer hydrogel sheath and synchronous droplet generation frequency with nozzle vibration, the DIS processes in this work were uniformly carried out under Mode 3.

The stability of structured microfibers produced by DIS method

To examine the stability of structured microfibers produced by DIS method, the Janus-beads-embedded microfibers (MF1) presented in Figure 4b and 4c were stored in 0.5 wt% $CaCl_2$ solution for 254 days. After storage, the retained microfibers (MF2) were tested to verify the structural stability. As shown in Figure S18a and S18b, the hydrogel sheath of MF2 kept intact and continuous, while the embedded beads maintained the Janus microstructures. More important, embedded Janus beads of MF2 maintained the original dimensions on the whole when compared to those of MF1, as shown in Figure S18c. Therefore, it was revealed that the

structured microfibers produced by the DIS method possessed outstanding stability in terms of the microstructures and dimensions.

The upper and lower limit of the diameters of embedded droplets in produced microfibers

In order to accurately obtain the diameters of embedded droplets, only the spherical droplets were taken into consideration here. For the DIS process with a fixed coaxial spinning nozzle (inner needle: 30G, outer needle: 21G), the upper limit (UL) and lower limit (LL) of spherical droplet diameters were 848.6μm (process parameters: Q_o = 120μL/min, Q_i = 58μL/min, f = 3Hz) and 99.9μm (process parameters: Q_o = 30μL/min, Q_i = 0.5μL/min, f = 15Hz), respectively. To obtain the UL of spherical droplet diameters, Q_o was kept as 120μL/min to form hydrogel knots with sufficient dimensions. The maximum size of spherical droplets containable in hydrogel knots was determined by adjusting Q_i. As the f increased, the value of UL decreased accordingly due to the size decrease of hydrogel knots, as shown in Figure S19a. To obtain the LL of spherical droplet diameters, Q_i was adjusted under the premise of stable droplet formation, with Q_o kept as 30μL/min. It was concluded that LL of spherical droplet diameters decreased as f increased, as shown in Figure S19b, due to the increasing interfacial shearing force applied on the inner phase. The minimum value of droplet diameters was measured when f was set as 15Hz. Further increasing f would lead to the increase in the diameter polydispersity of embedded droplets, owing to the increased fluidic disturbance introduced by nozzle vibration.

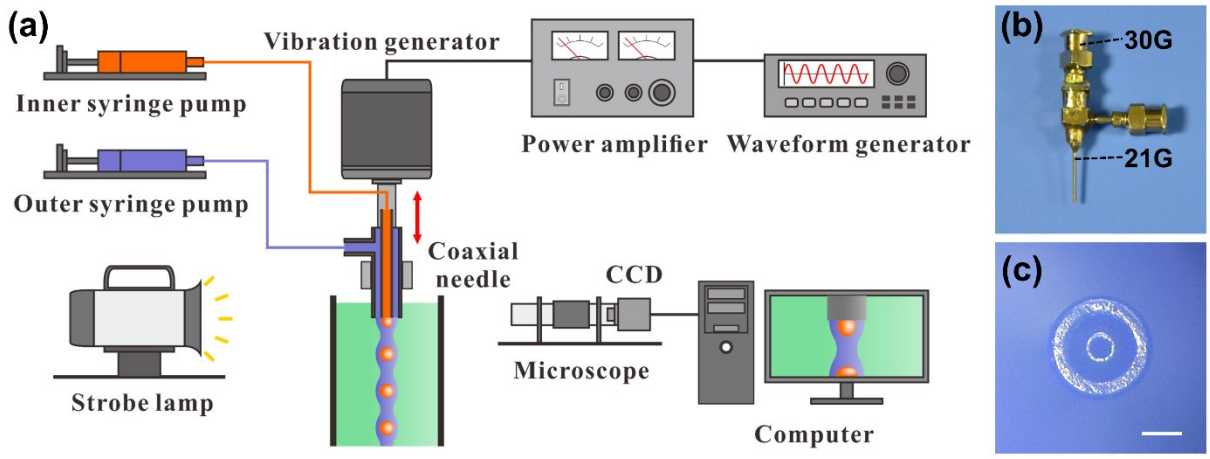

Figure S1. a) Schematic diagram of the experimental system for programmable DIS process. b) Photograph of the coaxial spinning nozzle. c) Stereomicroscopy image of the nozzle outlet. Scale bar is 300 μm in c).

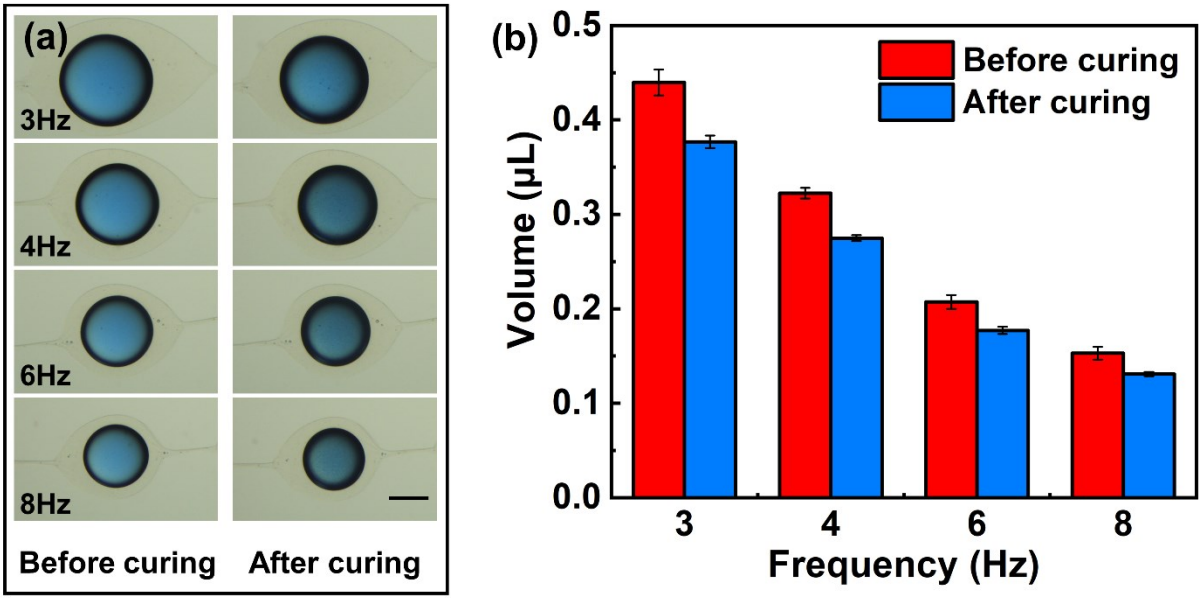

Figure S2. The volume variation of embedded droplets in microfibers after solidification. a) Bright-field microscopy images of embedded droplets before curing (left) and solidified beads after curing (right). b) Effect of UV-induced solidification on the volumes of embedded droplets generated under different vibration frequencies. Q_0 = 60 μL min^{-1}, Q_i = 10 μL min^{-1}, H = 1.272 mm. Scale bar is 200 μm in a).

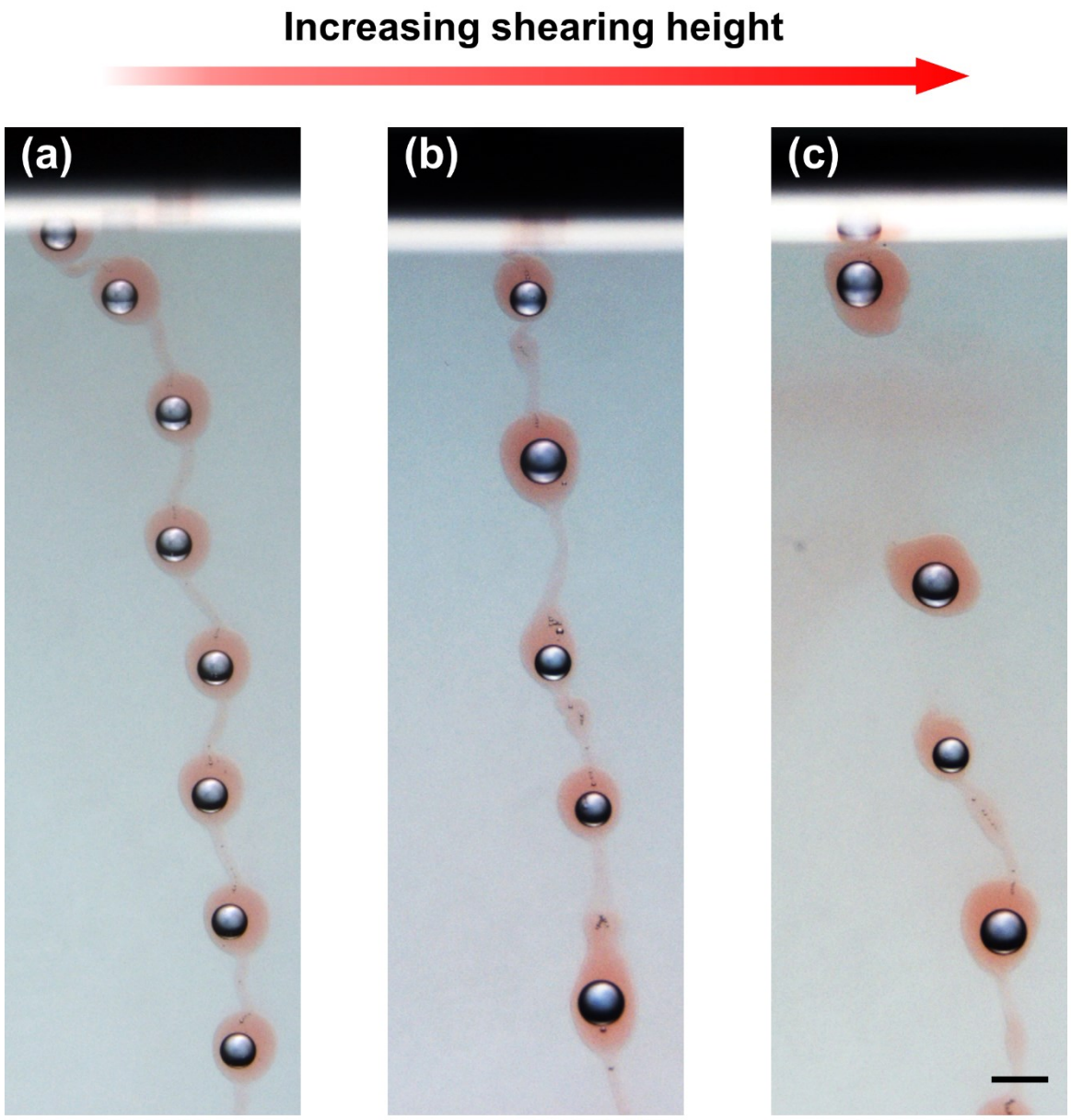

Figure S3. The morphology evolution of deformed hydrogel sheath with increasing shearing height. a) Generation of microfibers with uniform embedded droplets and regular knots-joints hydrogel sheath. Q_0 =30 μL min^{-1}, Q_i =5 μL min^{-1}, f = 5 Hz, H = 1.545 mm. b) Generation of microfibers with non-uniform embedded droplets and irregular hydrogel sheath. H = 2.127 mm. c) Generation of microfibers with non-uniform embedded droplets and fractured hydrogel sheath. H = 2.382 mm. Scale bar is 500 μm.

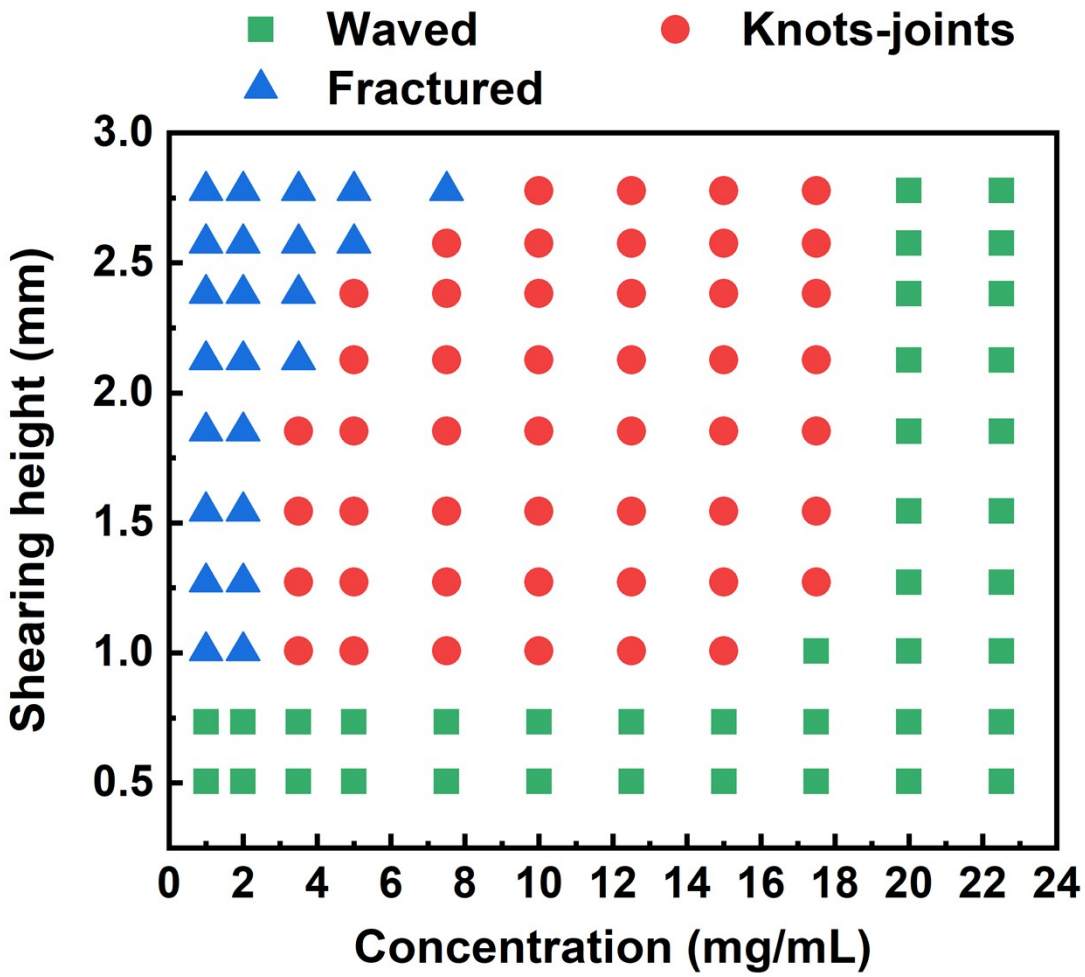

Figure S4. Influence of the alginate concentration and shearing height on the morphology of hydrogel microfibers. Q =30 μL min^{-1}, f = 4 Hz (Q is the flow rate of alginate solution).

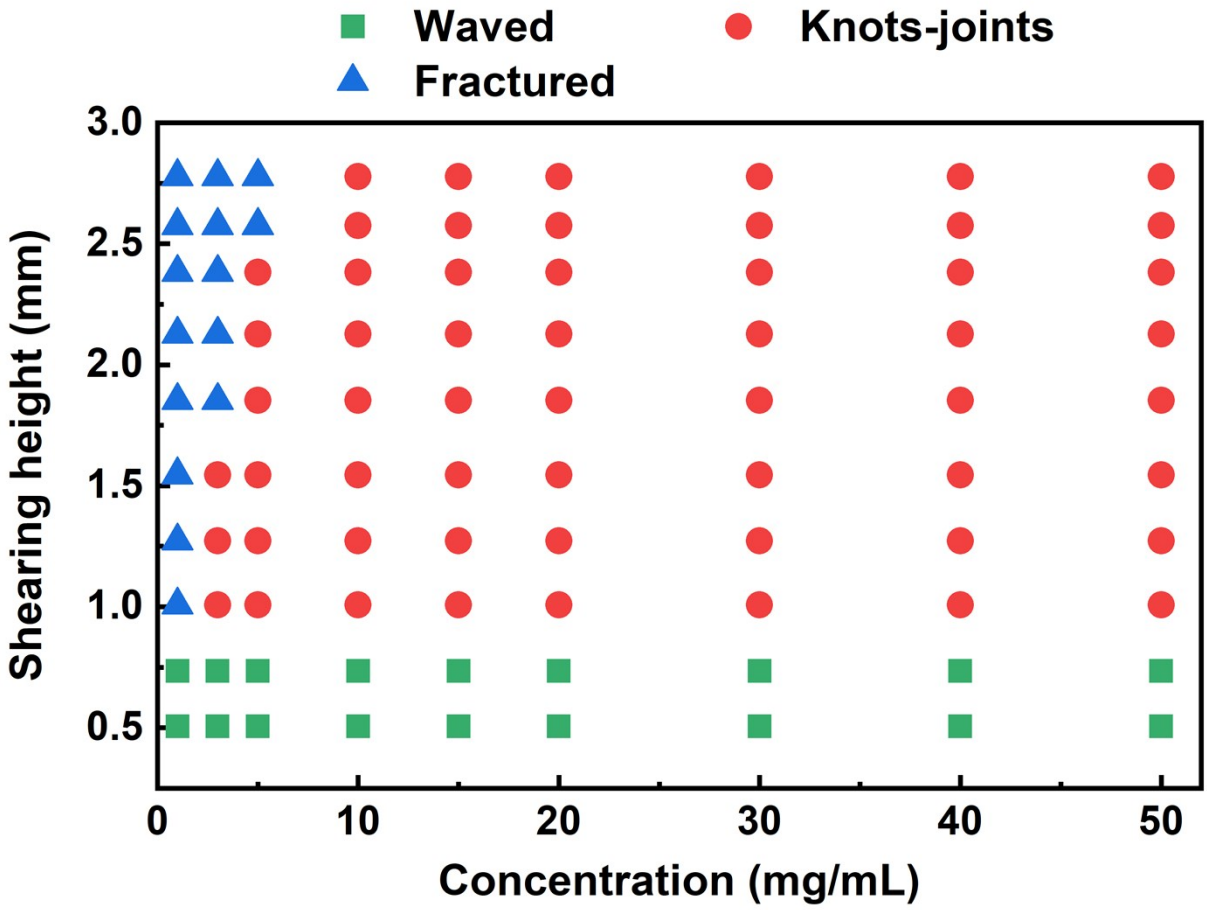

Figure S5. Influence of the $CaCl_2$ concentration and shearing height on the morphology of hydrogel microfibers. Q =30 μL min^{-1}, f = 4 Hz.

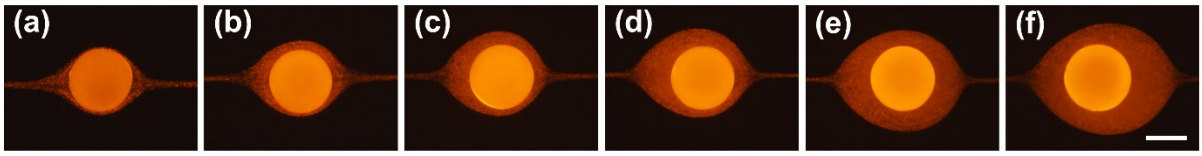

Figure S6. Influence of the outer flow rate on the dimension of hydrogel knots. a)-f): Q_0 =10, 20, 30, 40, 60, 80 μL min^{-1}. Q_i = 5 μL min^{-1}, f = 4 Hz, H = 1.272 mm. Scale bar is 200 μm.

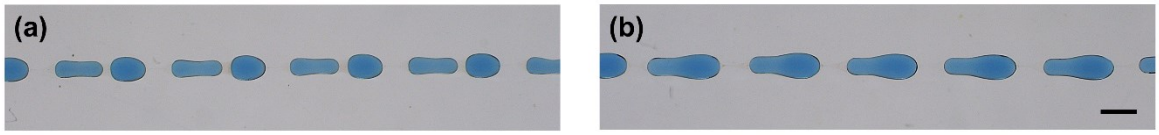

Figure S7. Stereomicroscopy images of DIS-produced microfibers encapsulating a) twinned (Q_0 = 60 µL min^{-1}. Q_i = 60 µL min^{-1}, f = 2 Hz, H = 1.272 mm) and b) clavated particles (Q_0 = 60 µL min^{-1}. Q_i = 120 µL min^{-1}, f = 4 Hz, H = 1.007 mm). Scale bar: 1 mm.

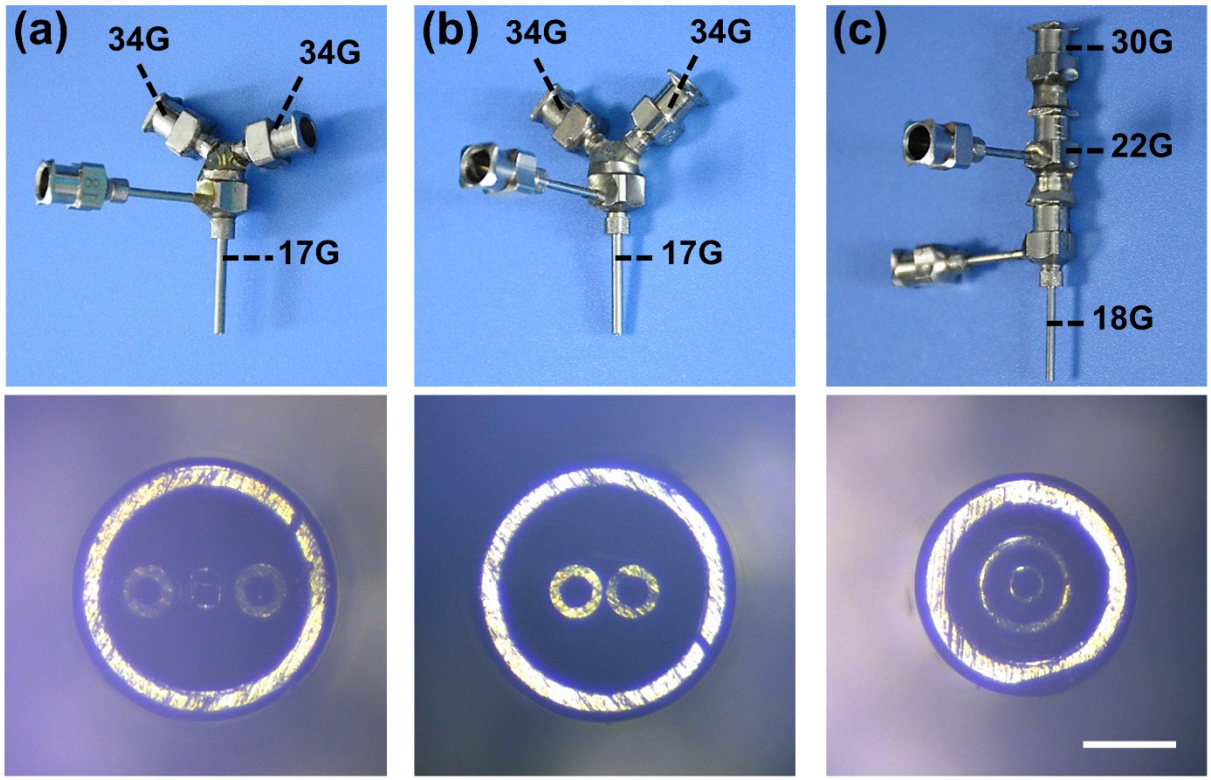

Figure S8. Configurations of spinning nozzles applied for the generation of deformed microfibers embedded with a) dual droplets, b) Janus droplets and c) core-shell capsules. Scale bar is 500 μm.

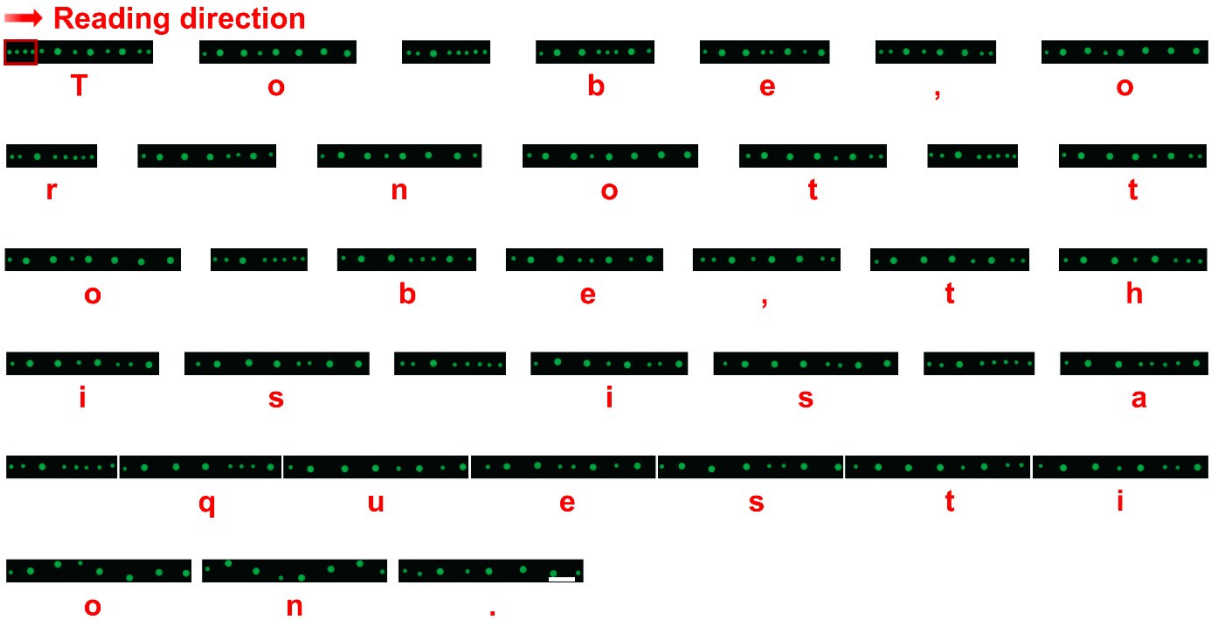

Figure S9. Fluorescent images of the encoding patterns in volume-encoded microfibers storing a complete drama line. Q_0 = 100 μL min^{-1}, Q_i = 10 μL min^{-1}. Scale bar is 2 mm.

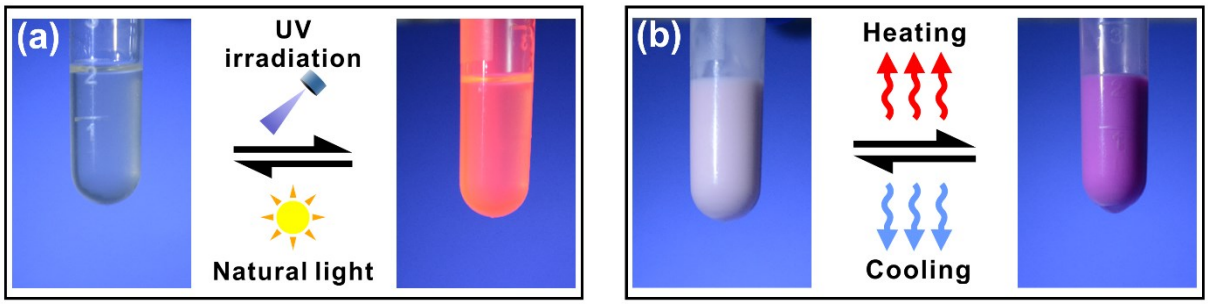

Figure S10. a) UV responsiveness and b) temperature responsiveness of two kinds of commercial security printing inks.

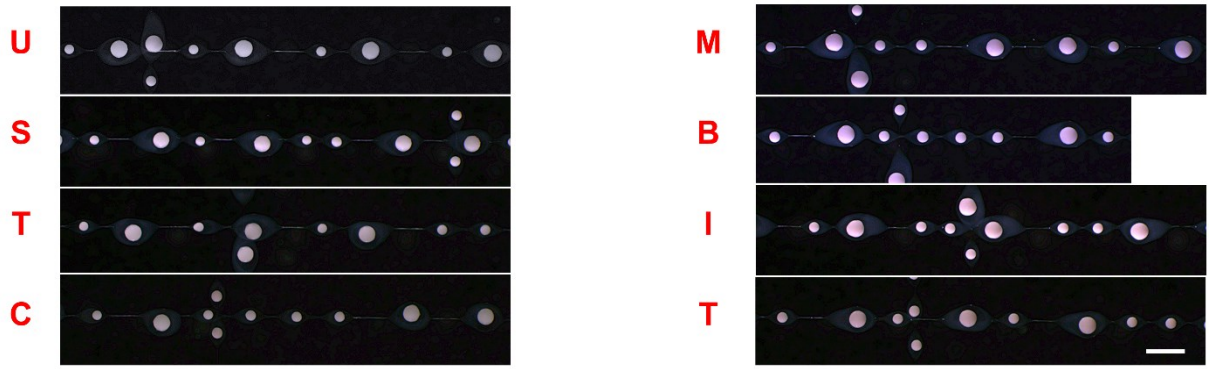

Figure S11. Stereomicroscopy images of the UV-responsive microfibers encoded with letter U, S, T, C, and temperature-responsive microfibers encoded with letter M, B, I, T. Q_0 = 100 μL min^{-1}, Q_i = 15 μL min^{-1}. Scale bar is 1 mm.

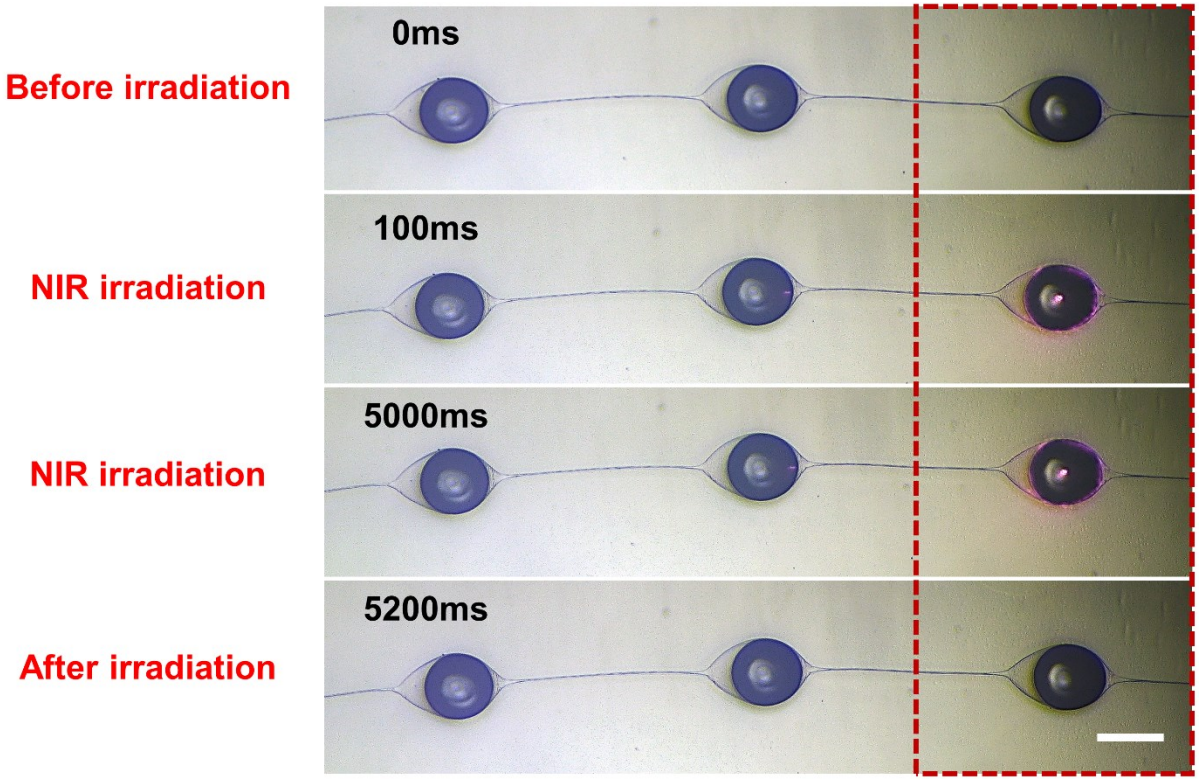

Figure S12. Stereomicroscopy images of HFC-embedded microfibers without dispersed MNPs under focused NIR irradiation. Q_o = 60 μL min^{-1}, Q_i = 15 μL min^{-1}, f = 6 Hz. Scale bar is 500 μm.

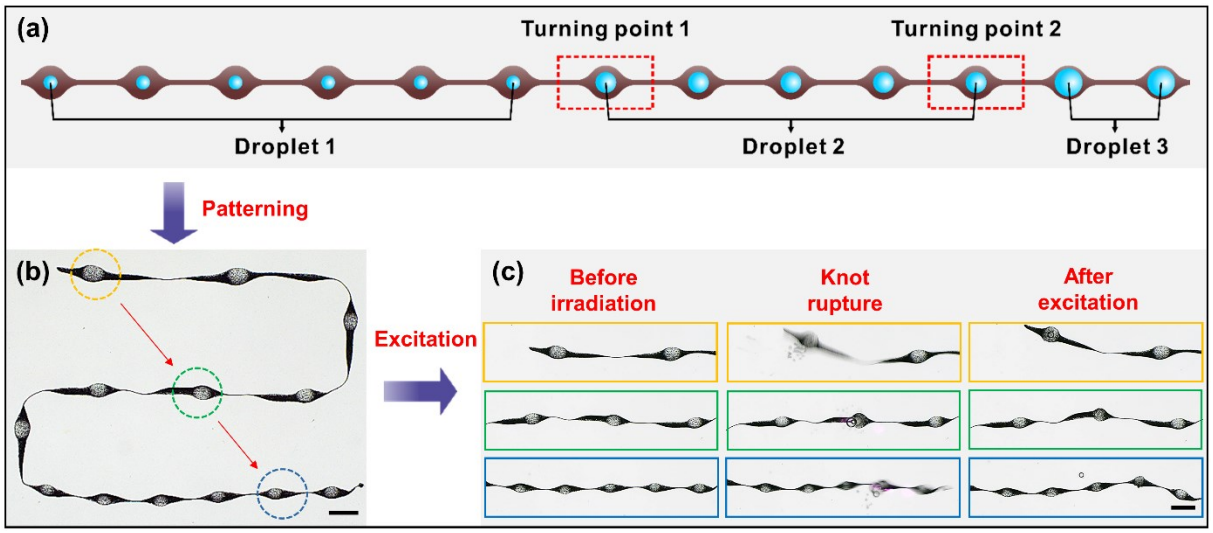

Figure S13. Sequential excitation of HFC droplets embedded in patterned volume-encoded microfibers. a) schematic diagram of the designed volume-encoded microfibers, b) Patterning and c) sequential excitation for the volume-encoded microfibers on the plane. Q_o = 60 μL min^{-1}, Q_i = 15 μL min^{-1}. Scale bars are 1mm in b) and c).

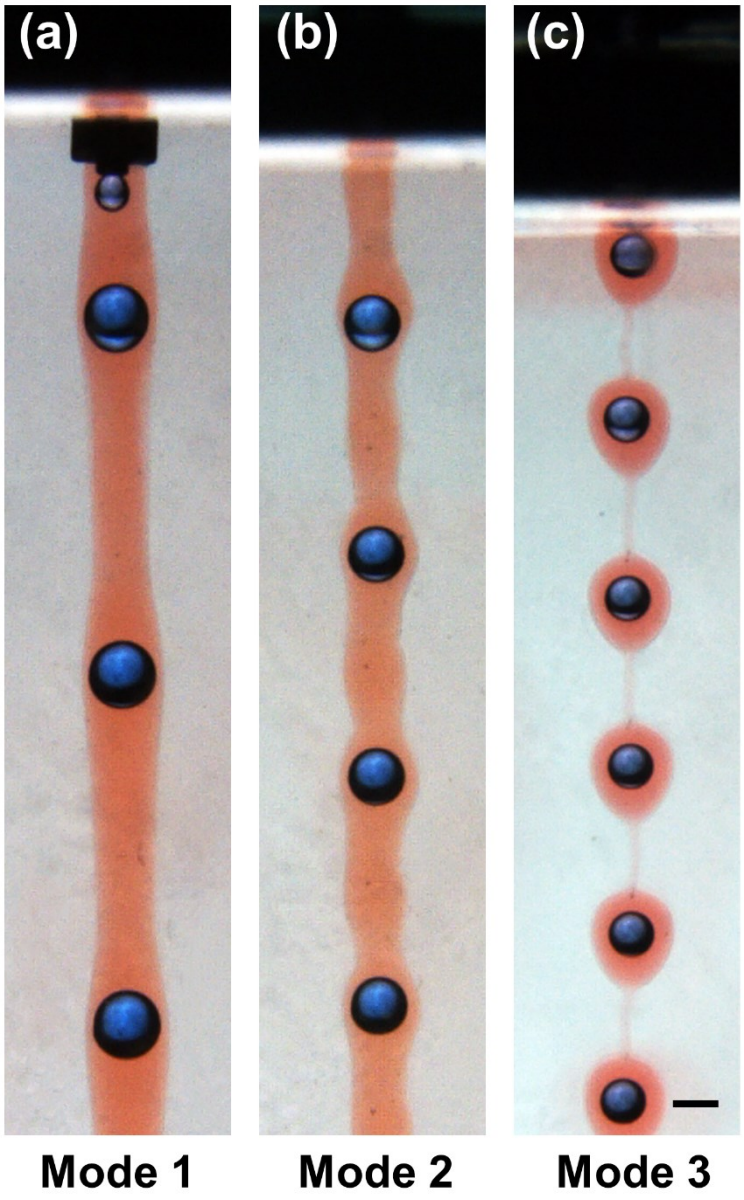

Figure S14. Three spinning modes in DIS process. a) Mode 1: passive breakage of inner phase without vibration of spinning nozzle; b) Mode 2: Asynchronous active breakage of inner phase with insufficient shearing height *H*. c) Mode 3: Synchronous active breakage of inner phase with sufficient shearing height *H*. Q_o = 60 μL min^{-1}, Q_i = 10 μL min^{-1}. Scale bars is 500 μm.

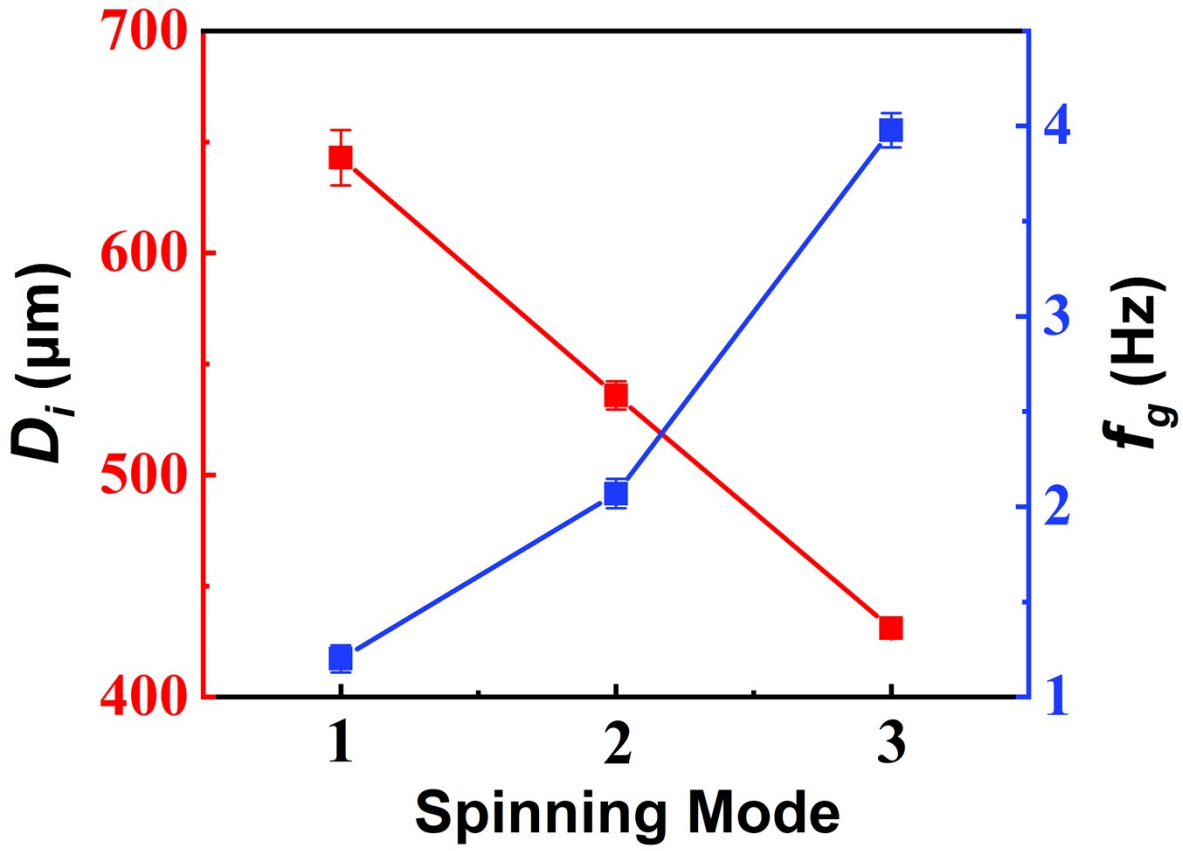

Figure S15. The measured diameters D_i and theoretical generation frequency f_g of embedded droplets under three spinning modes. Q_o = 60 μL min^{-1}, Q_i = 10 μL min^{-1}.

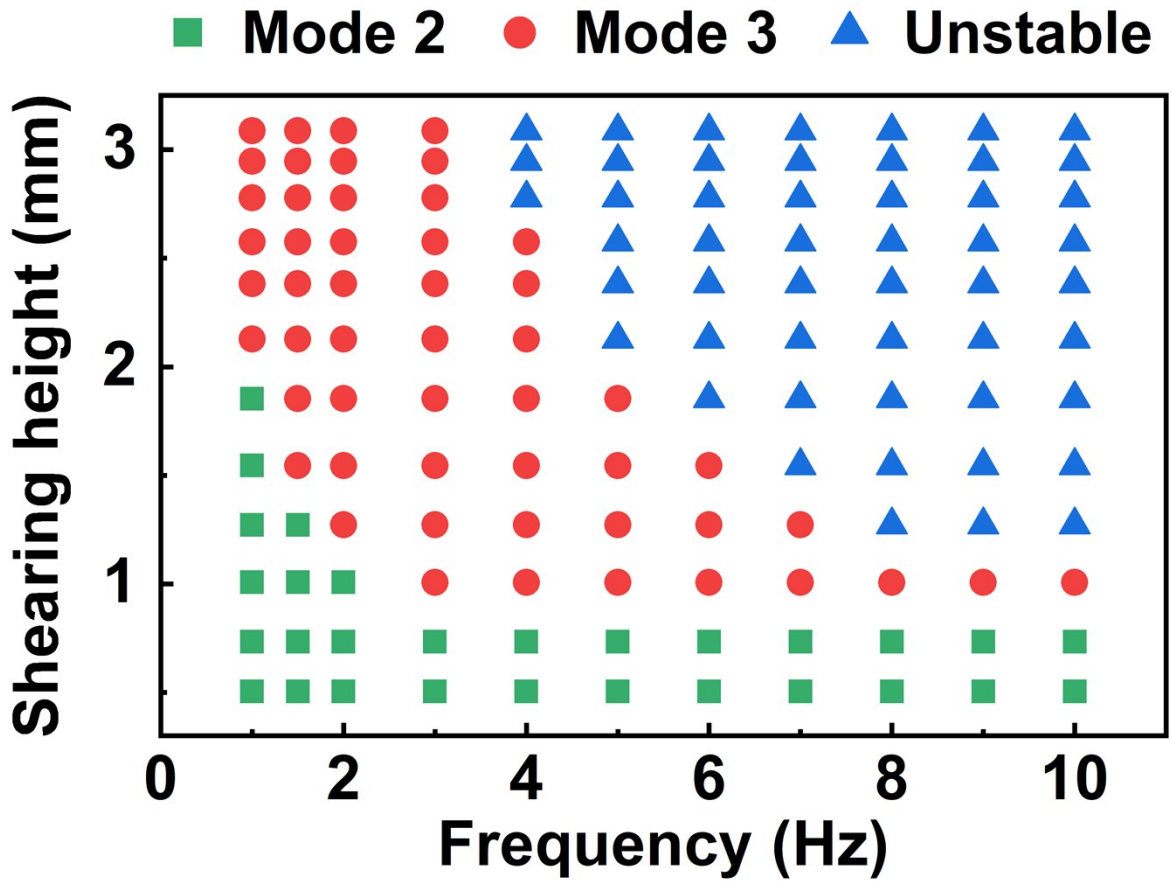

Figure S16. Effects of vibration frequency and shearing height on the spinning modes in DIS process. Q_0 =30 μL min^{-1}, Q_i =5 μL min^{-1}.

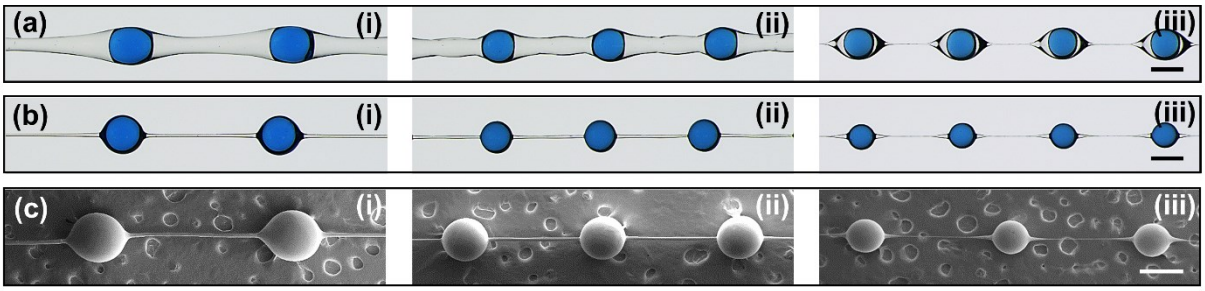

Figure S17. Stereomicroscopy images of a) hydrated and b) dehydrated droplet-embedded microfibers generated under i) Mode 1, ii) Mode 2, and iii) Mode 3. c) SEM images of dehydrated droplet-embedded microfibers generated under three spinning modes. Q_o = 60 μL min^{-1}, Q_i = 10 μL min^{-1}. Scale bars are 500 μm in a), b) and c).

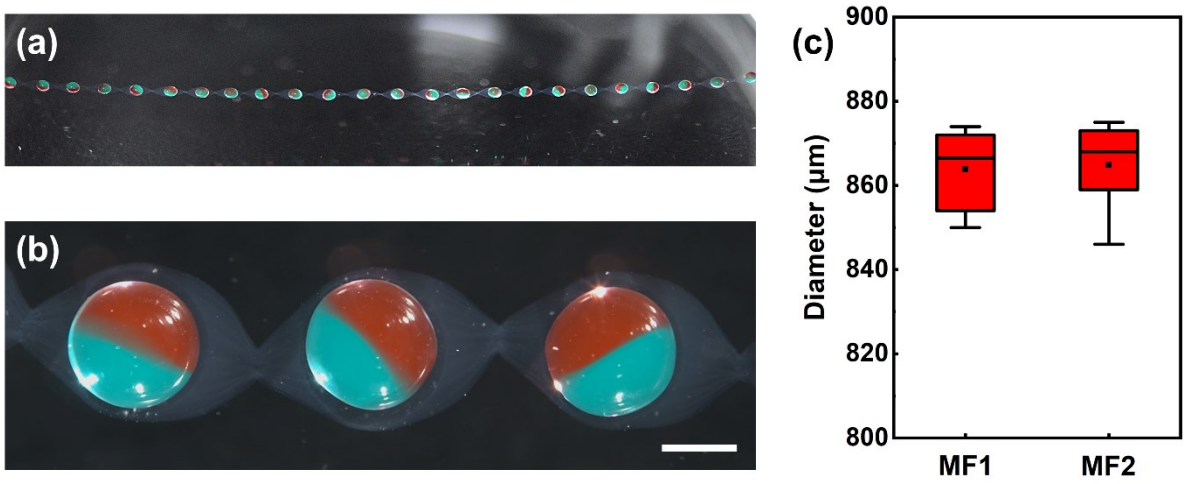

Figure S18. The stability of DIS-produced microfibers encapsulating Janus beads. a) The macroscopic appearance of Janus-beads-embedded microfiber (MF2) after 254 days of storage in 0.5 wt% $CaCl_2$ solution. b) Stereomicroscopy image exhibiting the intact microstructure of MF2 after storage. c) The bead dimensions of MF2 and the same microfibers before storage (MF1). Scale bars are 500 µm in b).

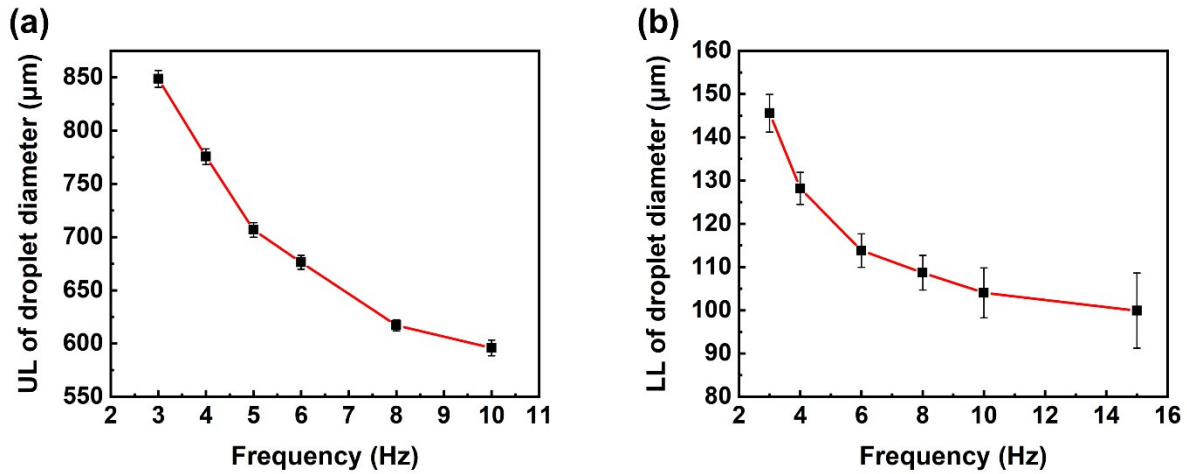

Figure S19. The influence of vibration frequency on a) the upper limit (UL) and b) lower limit (LL) of the diameters of containable spherical droplets.

Supplementary Movies

Movie S1. Morphology evolution of droplet-embedded microfibers with increasing shearing height.

Movie S2. Consecutive generation of droplet-embedded microfiber encoded with letter M.

Movie S3. Decryption of two-dimensional encrypted network by UV irradiation and temperature increase, respectively.

Movie S4. Sequential excitation of embedded HFC droplets along a diagonal path using focused NIR irradiation.